Biochemical and Biophysical Research Communications 661 (2023) 89–98

Contents lists available at ScienceDirect

Biochemical and Biophysical Research Communications

journal homepage: www.elsevier.com/locate/ybbrc

Non-thermal disruption of β-adrenergic receptor-activated Ca^{2+} signalling and apoptosis in human ES-derived cardiomyocytes by microwave electric fields at 2.4 GHz

Catrin F. Williams [a, d], Catherine Hather [b], Jainaba Sallah Conteh [c], Jingjing Zhang [b], Raluca G. Popa [c], Anthony W. Owen [c], Cara L. Jonas [c], Heungjae Choi [a], Rhian M. Daniel [b], David Lloyd [a, d], Adrian Porch [a, **], Christopher H. George [c, *]

[a] School of Engineering, Cardiff University, Wales, UK
[b] School of Medicine, Cardiff University, Wales, UK
[c] Medical School, Swansea University, Wales, UK
[d] School of Biosciences, Cardiff University, Wales, UK

ARTICLE INFO

Article history:
Received 30 March 2023
Accepted 15 April 2023
Available online 17 April 2023

Keywords:
Microwaves
Electric field
Non-thermal
Cardiomyocytes
Calcium
Apoptosis

ABSTRACT

The ubiquity of wireless electronic-device connectivity has seen microwaves emerge as one of the fastest growing forms of electromagnetic exposure. A growing evidence-base refutes the claim that wireless technologies pose no risk to human health at current safety levels designed to limit thermal (heating) effects. The potential impact of *non-thermal* effects of microwave exposure, especially in electrically-excitable tissues (e.g., heart), remains controversial. We exposed human embryonic stem-cell derived cardiomyocytes (CM), under baseline and beta-adrenergic receptor (β-AR)-stimulated conditions, to microwaves at 2.4 GHz, a frequency used extensively in wireless communication (e.g., 4G, Bluetooth™ and WiFi). To control for any effect of sample heating, experiments were done in CM subjected to matched rates of direct heating or CM maintained at 37 °C. Detailed profiling of the temporal and amplitude features of Ca^{2+} signalling in CM under these experimental conditions was reconciled with the extent and spatial clustering of apoptosis. The data show that exposure of CM to 2.4 GHz EMF eliminated the normal Ca^{2+} signalling response to β-AR stimulation and provoked spatially-clustered apoptosis. This is first evidence that non-thermal effects of 2.4 GHz microwaves might have profound effects on human CM function, responsiveness to activation, and survival.

© 2023 The Authors. Published by Elsevier Inc. This is an open access article under the CC BY license (http://creativecommons.org/licenses/by/4.0/).

1. Introduction

The rapid increase in wireless connectivity of electronic devices (e.g., the Internet of Things (IoT)) has seen microwave-range electromagnetic fields (EMF) emerge as one of the fastest growing forms of electromagnetic exposure [1]. The ubiquity of 'human-made' environmental microwaves (ranging from 1 to 30 GHz and encompassing key designated frequency bands for industrial, medical, and scientific applications) lends urgency to the need to add knowledge on their potential impact on human biology and health. Microwaves heat polar molecules (e.g., water) through a dielectric relaxation, with the absorbed microwave energy being dissipated as heat. In order to prevent potential heating effects, European safety standards limit all domestic microwave-emitting devices (e.g., mobile phones) to an absorption rate of <2 mW/g [2]. Different interpretations of available data have led to different national guidelines on microwave EMF safety limits [3].

However, a growing evidence-base refutes the claim that widespread deployment of microwave-frequency wireless technologies (e.g. '4G') poses no risk to human health at currently permitted safety levels [4–6]. Studies involving mobile phones, in particular, are prone to inherent issues such as changing technologies and phone use habits, in addition to low numbers for the unexposed control group. Several questions relating to the safety of microwaves at these frequencies remain unresolved [2,3,7].

* Corresponding author. Medical School, Faculty of Medicine, Health and Life Sciences, Swansea University, Singleton Park Campus, Swansea, SA2 8PP, Wales, UK.
** Corresponding author. School of Engineering, Cardiff University, Queen's Building, 14-17 The Parade, Newport Road, Cardiff, CF24 3AA, Wales, UK.
E-mail addresses: porcha@cardiff.ac.uk (A. Porch), christopher.george@swansea.ac.uk (C.H. George).

https://doi.org/10.1016/j.bbrc.2023.04.038
0006-291X/© 2023 The Authors. Published by Elsevier Inc. This is an open access article under the CC BY license (http://creativecommons.org/licenses/by/4.0/).

Microwave EMF impacts on embryonic development in zebrafish [8], chicks [9] and humans [10] and is also reported to disrupt the function of neurologic [11], cardiovascular [12–15], blood [16,17] and other biological systems [18]. The effects of microwaves might be of particular relevance in the context of electrically-excitable tissues, where evidence exists for the disruption of ion handling in *in vitro* culture systems of brain and heart cells [19–22]. Although the majority of the effects reported are presumed to be mediated by a thermal (heating) effect of EMF, the contribution of non-thermal mechanism(s) to downstream effects of EMF remains controversial [7,23–25].

In this proof-of-concept study, we demonstrate the functional impact of non-thermal effects of the electric field component of microwaves at a major frequency band used extensively in 4G, Bluetooth™ and WiFi communications (i.e., 2.4 GHz) on human embryonic stem-cell derived CM.

2. Materials & methods

2.1. Materials

Human embryonic stem-cell derived CM (Cytiva™) were obtained from GE Healthcare. All Cytiva™ used in this study were from a single batch (7396634) in which CM comprise 74% of the total cellular component [26,27].

All chemicals were the highest quality available from Sigma unless stated. 10 kD and 70 kD dextrans (Dex-10 and Dex-70) conjugated to tetramethyl-rhodamine (TMR) were from Molecular Probes. Staurosporine was from Merck. All cell culture reagents were Gibco brand from ThermoFisher except for Matrigel which was obtained from Corning Biosciences. Other materials were obtained from sources as described below.

2.2. Experimental design

CM were randomly allocated to three experimental groups (EMF-exposure ('EMF'); heating only ('Heat'); control ('Ctrl')). After exposure to these conditions, CM were subsequently randomized again prior to the addition of isoproterenol ('ISO') or to vehicle-only (media) control ('Veh'). To prevent EMF-induced heating raising the temperature of the bulk media to above 37 °C during the 1-min exposure to microwave EMF, CM in the 'EMF' group were cooled to 28 °C immediately prior to the application of microwaves. To control for this heating effect, experiments were done in CM-populations cooled to 28 °C and then heated to 37 °C using a programmable heating platform that raised the temperature of the sample at the precise rate measured experimentally in the EMF group ('Heat'). To control for any heating effect resulting from either direct heating or by EMF exposure, control experiments were also done in which CM were maintained at 37 °C throughout the experimental protocol ('Ctrl'). The experimental design is shown in Fig. 1A. All data acquired were analysed by operators blinded to the nature of experimental conditions under test. 'N' defines the number of discrete CM tubes studied in independent experiments and 'n' denotes the number of sub-tubular regions (see Supplementary Fig. 1S).

2.3. Cardiomyocyte (CM) network formation

CM were seeded in silicone chambers adhered to matrigel-coated glass in RPMI1640 medium supplemented with B27 [26,27]. Before exposure to 'Ctrl', 'Heat' or 'EMF' conditions, CM were transferred from this medium (free [Ca^{2+}] approximately 0.4 mM) into indicator-free Leibovitz (L-15) medium (free [Ca^{2+}] approximately 1.3 mM) and loaded with fluo-4 Ca^{2+}-sensitive reporter [26,27]. All data were acquired from tubular-like CM structures (Fig. 1B and Supplementary Movie 1).

2.4. Microwave instrumentation

Microwave electric (E-) and magnetic (H-) fields were separated using a TM_{010} mode cylindrical resonant cavity, with samples exposed to the axial E-field (where H is close to zero) [28,29]. The equipment delivered an output power of 19 W rms at 2.4 GHz (at resonance with $|S_{11}|$ of −35 dB) via 10 ms pulses in a 50% duty cycle for a duration of 60 s. The temperature of the aqueous environment in the immediate vicinity of CM was monitored continuously using a fluoroptic sensor (Luxtron, LumaSense Technologies, Santa Clara, CA, USA) which does not interact with the applied microwave fields [30].

2.5. COMSOL multiphysics simulation

To visualise E- and H-field distributions within the resonant cavity, and to calculate the field intensity applied to sample cells under test, 3D finite-element simulation was carried out using COMSOL Multiphysics v4.4 [31]. The simulation model replicated the experimental conditions: an aluminium microwave cylindrical cavity (relative permittivity (ε_r), 1; electrical conductivity (σ), 3.774e7 S/m) with an input coaxial coupling port (N-type connector), polystyrene confocal culture dish (ε_r, 2.5; σ, 0) with silica-glass coverslip (ε_r, 5; σ, 1e-14 S/m), CM contained in a silicone chamber (ε_r, 3.5; σ, 1e-12 S/m), and L-15 (aqueous) medium (ε_r, 80-j*10; σ, 5.5e-6 S/m) [26]. The simulated resonant frequency of TM_{010} mode was 2.4 GHz (Fig. 1C).

2.6. Ca^{2+} imaging and CM frequency stimulation via β-AR activation

Baseline Ca^{2+} oscillations were recorded in CM maintained at 37 °C in phenol-red-free L-15 medium using resonant-scanning confocal microscopy (Leica SP5) [26,27,32] (Supplementary Movie 2). In some experiments the non-selective β-AR agonist, isoproterenol, was used to elicit a sustained increase in oscillatory rate (ISO; 30 nM, prepared via the dilution, in L-15 medium, of a 10 mM ISO stock containing 30 mM ascorbate). To control for the addition of ISO, vehicle-only experiments were done (Veh; L-15 medium containing 100 nM ascorbate). Following simultaneous imaging of brightfield (contractility) and fluorescence (Ca^{2+}) signals, CM-containing chambers were returned to 37 °C/5% CO_2 incubation for 4 h prior to quantification of apoptosis.

2.7. Ca^{2+} signal analysis

Imaging datasets were segmented into symmetric 4 × 4 regional grids (Supplementary Fig. 1S) and fluorescent time-series data corresponding to fluo-4-dependent Ca^{2+} signals were analysed using SALVO software [26,27,32]. An eleven-parameter output provided a quantitative description of temporal and amplitude features of CM Ca^{2+} signals (Supplementary Fig. 1S).

2.8. Quantification of the extent and spatial clustering of apoptosis

Apoptosis was measured by quantifying the extent of nuclear DNA fragmentation in CM 4 h after Ca^{2+} imaging using the terminal deoxynucleotidyl transferase dUTP nick end labelling (TUNEL) method as per manufacturer's instructions (DeadEnd, Promega). Nuclei were counterstained with propidium iodide (0.5 μM), samples were mounted under Prolong Gold (Invitrogen) and stored at 4 °C until analysis. In other experiments, staurosporine (1 μM, 4 h)

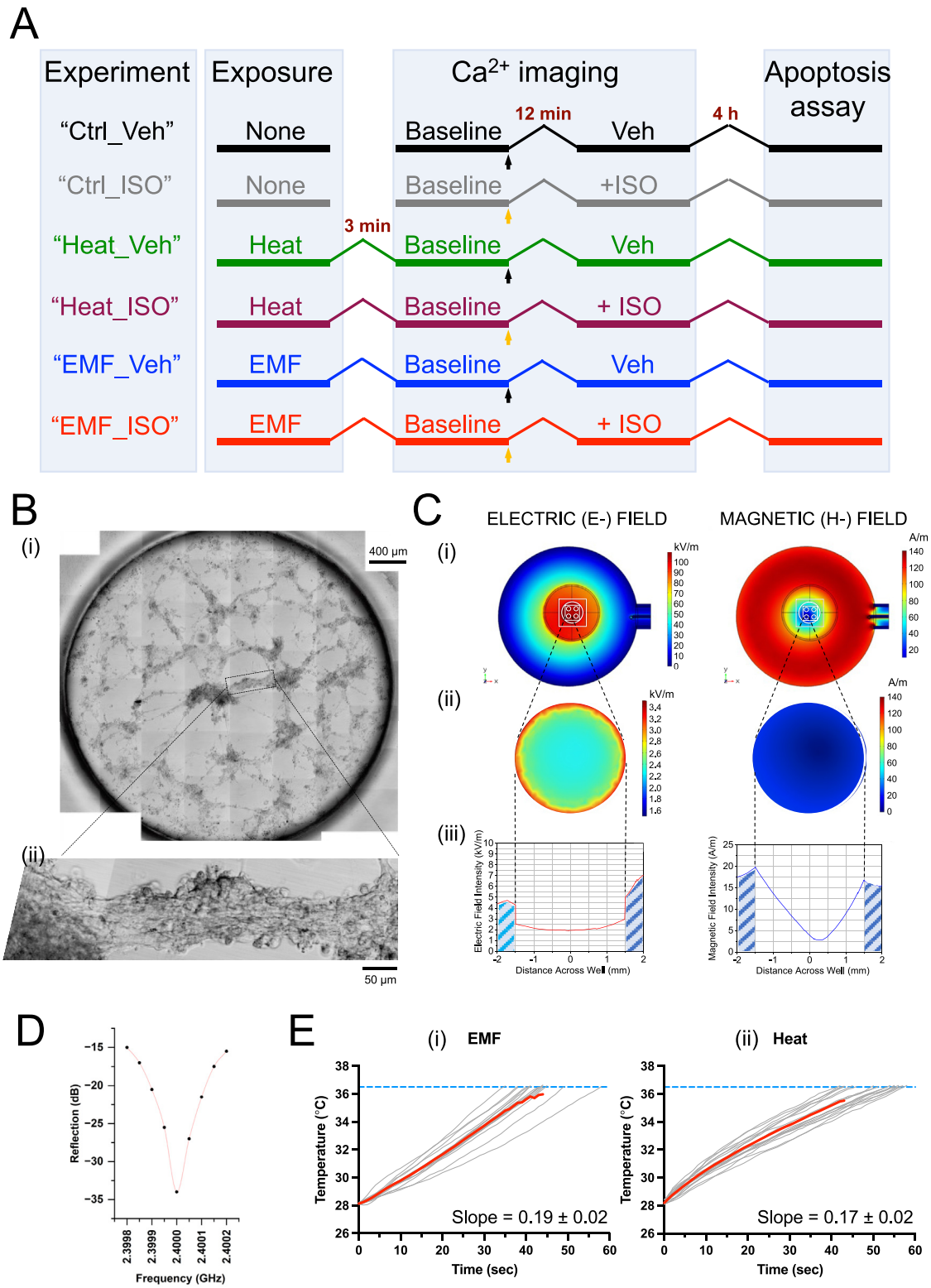

Fig. 1. CM networks, microwave instrumentation and experimental design. **(A)** Experimental design. Black and orange arrows denote addition of vehicle-only (Veh) or ISO (30 nM), respectively. **(B) (i)** Composite image of a typical CM network produced by tessellation of separate brightfield images (456 × 456 μm each). The boxed area is magnified in **(ii)** and depicts the 'tube-like' CM structures from which data were acquired. **(C)** Electric (E-) and magnetic (H-) field intensities (simulated using COMSOL) in the bulk resonant cavity **(i)** and in the plane of the CM **(ii)** and **(iii)**. **(D)** Resonance/frequency domain plot showing the maximum absorption of microwaves by the sample occurs at 2.4 GHz. **(E)** Rates of heating in 'EMF' and 'Heat' groups (N = 16 and 18, respectively). The average thermal profile (red) was calculated from data obtained from separate experiments (grey). (For interpretation of the references to colour in this figure legend, the reader is referred to the Web version of this article.)

was used to induce maximal apoptosis [33]. The spatial clustering of TUNEL-positive nuclei was done using digitized confocal images and a maximum-likelihood probability density function programmed in MatLab (Mathworks) [34]. The maximum and minimum extent of spatial clustering of apoptotic nuclei was assigned '1' and '0', respectively.

2.9. Assessing CM membrane intactness using fluorescent-conjugated dextrans

Endogenous CM fluorescence at 575 nm was imaged following excitation using a 543 nm HeNe laser. CM were then equilibrated for 5 min with TMR-conjugated Dex-10 and Dex-70 (ex_{max} 555 nm/em_{max} 580 nm) used at 5 μM to avoid aggregation. Dex-10 or Dex-70-incubated CM were then subject to heating-only or EMF exposure for 1 min and TMR fluorescence was continuously recorded over a subsequent 3 min period. The maximum intracellular accumulation of Dex-10 and Dex-70 was determined following the permeabilization of CM surface membrane using saponin (0.01% (w/v) in L-15 medium).

2.10. Statistical analysis

All data were tested for normal distribution. No log-transformation of data was done. Pair-wise comparisons of data within the same group (e.g., same CM tube before and after the addition of ISO or vehicle) were compared using paired student's T-test or Mann-Whitney test for normal or non-normally distributed data, respectively. For comparison of more than two groups, ANOVA or Kruskal-Wallis was used if the data were normally or non-normally distributed, respectively. Where gateway criteria for post-hoc testing were met, Holm-Sidak (normal) or Dunn (non-normal) testing was done. For comparison of more than two groups with two variables (i.e., exposure condition and ISO/vehicle addition), two-way ANOVA was used. Correlation analysis of Ca^{2+} signalling parameters was done by calculating Spearman correlation co-efficients. All statistical analysis was done using MatLab (Mathworks, vFeb22), and Prism (v9.0, GraphPad).

3. Results

Cytiva™ CM formed spontaneously-organised networks of contractile 'tubes' (Fig. 1B; Supplementary Movies 1 and 2) which were exposed for 1 min to uniform E-field strength (around 2 kV/m; Fig. 1C (left column)) and negligible H- field strength (<5 A/m; Fig. 1C (right column)) at a frequency of 2.4 GHz (Fig. 1D). These conditions produced a linear rate of heating of the aqueous environment immediately surrounding the CM of 0.19 ± 0.02 °C/s (Fig. 1E (i)). To control for this thermal effect of EMF, this heating profile was recreated precisely using a programmable heating platform, in the absence of any extrinsic E- or H- fields (0.17 ± 0.02 °C/s; Fig. 1E (ii)).

SALVO was used to generate an eleven-parameter description of the temporal and amplitude features of Ca^{2+} signalling (see Supplementary Fig. 1S) in CM under baseline conditions following exposure to 'Ctrl', 'Heat' or 'EMF' regimes. Baseline Ca^{2+} signalling parameters including synchronisation, an index of the extent of functional coupling between CM (Supplementary Movie 2), were comparable in all three experimental groups (Table 1). The rate of Ca^{2+} release and the rate of Ca^{2+} decay was equivalently changed in 'EMF' and 'Heat' groups when compared with CM maintained at 37 °C ('Ctrl') (Table 1).

ISO (30 nM) was used to stimulate β-AR-mediated Ca^{2+} signalling in CM previously exposed to Ctrl, Heat or EMF conditions (Fig. 1A). Paired assessments of baseline Ca^{2+} signalling, and following a 12-min incubation in ISO, showed that ISO extensively modulated Ca^{2+} signalling in control CM, including a characteristic increase in oscillatory frequency (Fig. 2A, Ctrl and 2B). There were also significant post-ISO changes in Ca^{2+} signalling in those CM exposed to heating alone, but oscillatory frequency remained unchanged in this group (Fig. 2A, Heat and 2B)). Remarkably, CM exposed to EMF did not exhibit any response in Ca^{2+} signalling following the addition of ISO and no Ca^{2+} signalling parameters were changed by ISO (Fig. 2A, EMF and 2B).

An association between disrupted Ca^{2+} signalling and susceptibility to apoptosis has been reported in CM [35]. Since EMF eliminated the response of CM to β-AR stimulation (Fig. 2), we explored whether this translated into enhanced sensitivity of CM to apoptosis (Fig. 3A). The addition of ISO to 'Heat'-treated CM resulted in levels of apoptosis comparable to that determined in vehicle-only experiments (6.7% versus 7.7%, respectively; Fig. 3B (i)). However, ISO addition to CM exposed to EMF was associated with significantly increased levels of apoptosis, relative to the vehicle-only group (11% versus 7%; 53% relative increase) (Fig. 3B (i)). In control CM maintained at 37 °C, ISO at concentrations up to 100 nM had no measurable impact on the levels of apoptosis (Fig. 3B (ii)).

In all experimental groups, the extent of apoptosis was variable (Fig. 3B (i)). However, there was a pronounced right-shift in the distribution of data acquired from the post-ISO EMF group (Fig. 3C and D). To investigate the possibility that some CM within the tubular structures might be differentially susceptible to apoptosis following EMF exposure, we quantified the spatial distribution of

Table 1
Baseline Ca^{2+} signalling parameters in control, heat-only and EMF exposed CM.

Ca^{2+}-signalling parameter	Units	CONTROL (N = 20)			HEAT (N = 24)			EMF (N = 21)		
		Average	Min	Max	Average	Min	Max	Average	Min	Max
Synchronisation	%	65 ± 4	41.55	97.33	60 ± 2	42.32	83.02	61 ± 3	43.08	84.55
Frequency	Hz	0.64 ± 0.06	0.30	1.23	0.50 ± 0.03	0.27	0.83	0.54 ± 0.04	0.24	0.84
Temporal heterogeneity	a.u.	0.19 ± 0.03	0.05	0.53	0.31 ± 0.05	0.06	1.22	0.39 ± 0.07	0.06	1.25
Amplitude heterogeneity	a.u.	0.11 ± 0.02	0.04	0.34	0.12 ± 0.02	0.05	0.33	0.11 ± 0.02	0.03	0.47
Ca^{2+} spike amplitude	$\Delta F/F_0$	1.6 ± 0.13	0.66	3.08	1.92 ± 0.09	1.36	2.92	1.76 ± 0.09	0.75	3.24
Ca^{2+} spike duration	s	1.65 ± 0.13	0.81	2.72	1.77 ± 0.06	1.17	2.28	1.78 ± 0.11	1.18	2.88
Ca^{2+} spike area	a.u.	0.80 ± 0.10	0.22	2.40	0.97 ± 0.07	0.56	1.96	0.91 ± 0.12	0.33	1.70
Rate of Ca^{2+} release	ΔF/s	209 ± 23	73.90	484.43	129 ± 9***	66.92	230.63	139 ± 12**	52.54	260.24
Rate of Ca^{2+} decay	ΔF/s	−47.1 ± 5.1	−15.09	−98.07	−26.7 ± 1.9***	−13.42	−49.14	−26 ± 2***	−9.24	−43.20
Ca^{2+} decay noise	a.u.	50.1 ± 4.9	14.45	97.50	37.4 ± 2.7	18.34	74.90	37 ± 3	12.27	58.91
Inter-spike noise	a.u.	0.13 ± 0.01	0.05	0.24	0.14 ± 0.01	0.08	0.21	0.13 ± 0.1	0.09	0.19

CM characterised by intercellular synchronisation <40% and oscillatory frequency <0.2 Hz were excluded from analysis as these are indicative of poor cell-to-cell coupling and sub-optimal CM network formation. Parameters are described in Supplementary Fig. 1S and data are given as mean ± standard error of the mean (SEM), expressed to one or two significant figures. F, fluorescence; a.u., arbitrary units. **p < 0.01 and ***p < 0.001 compared with control group.

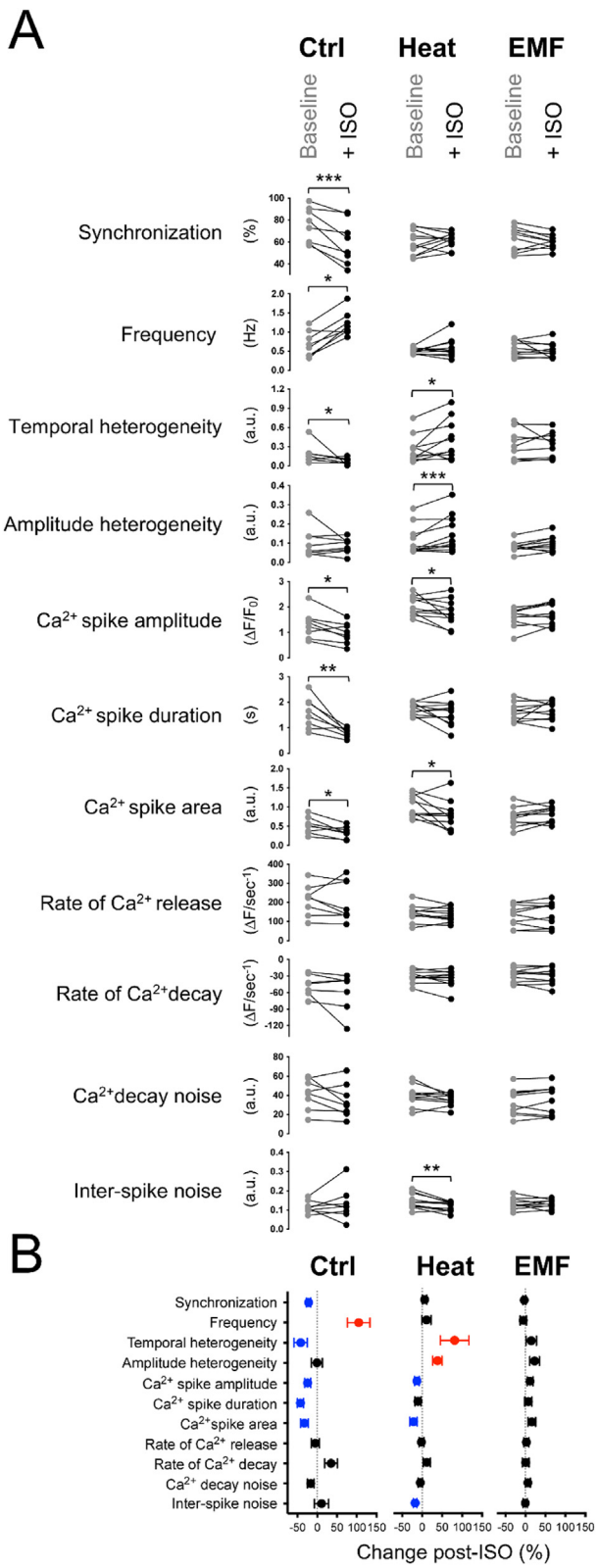

Fig. 2. The effect of heat or 2.4 GHz EMF on baseline and ISO-stimulated Ca^{2+} signalling. **(A)** Paired assessment of Ca^{2+} signalling parameters in CM under baseline conditions (grey) and following the addition of ISO (30 nM, 12 min) (black). Data were acquired from CM maintained under under control temperature conditions (Ctrl) or those exposed to heating only (Heat) or to EMF (EMF). Post-ISO data were normalised to separate experiments in which CM were exposed to vehicle-only addition (Veh; see Experimental Design, Fig. 1A). Where the addition of ISO stopped Ca^{2+} oscillations, data were excluded. Ctrl, N = 8; Heat, N = 11; EMF = 10 CM tubes. *, $p < 0.05$; **, $p < 0.01$; ***, $p < 0.001$. **(B)** Relative changes in Ca^{2+} signalling parameters following ISO addition were calculated from the data shown in **(A)**. Blue and red denote statistically significant reductions and increases, respectively ($p < 0.05$). (For interpretation of the references to colour in this figure legend, the reader is referred to the Web version of this article.)

apoptotic nuclei under these experimental conditions. The output of a probability density function, used previously to investigate cellular clustering in the post-infarct swine heart [34], showed significantly increased spatial clustering of apoptosis in EMF-exposed CM, when compared with those CM exposed to heating alone (clustering index of 0.37 versus 0.26, respectively) (Fig. 3E).

Previous work using bacteria has shown that microwaves at a power of around 5 W/g caused membrane poration [36]. Our finding that, under the experimental conditions used in the present study, baseline Ca^{2+} signalling in CM exposed to 2W/g EMF remained largely unchanged (Table 1) suggested strongly that the CM surface membrane remained intact. Corroborating this conclusion, experiments done using TMR-conjugated Dex-10 and Dex-70 revealed negligible accumulation of these fluorescent labels in CM following heating-only or EMF exposure (Fig. 4 and Supplementary Movie 3S).

The temporal and amplitude features of cellular Ca^{2+} oscillations are highly interconnected and the extent of disruption of these inter-relationships can be used as an index of CM dysfunction [26,27,35,37]. We hypothesised therefore that, even though there was no change in any discrete Ca^{2+} signalling parameter in the EMF-treated CM group in response to ISO (Fig. 2), the increased levels and spatial clustering of apoptosis determined in this group (Fig. 3) might be associated with alterations in the inter-relationships of these Ca^{2+} signalling parameters. Correlation analysis of the multi-parametric output from SALVO (Supplementary Fig. 1S) revealed extensive changes in the inter-relationships of Ca^{2+} signalling parameters in control, heating-only and EMF CM groups following ISO addition (Fig. 5A (i), (ii) and (iii), respectively). Directly comparing the data obtained from heat-treated or EMF-exposed CM with those from control CM showed that the nature and extent of changes in inter-parametric correlations following heating alone (Fig. 5B(i)) or EMF-exposure (Fig. 5B(ii)) were very different.

4. Discussion

The heart is the human body's largest bioelectrical source, and its normal function depends on the electrical and functional synchronisation of approximately three billion CM *in situ* [38]. This proof-of-concept study is the first to resolve a non-thermal effect of 2.4 GHz EMF on functionally-coupled human CM networks *in vitro*. A major objective of the work was to employ EMF at power sufficient to elicit a pronounced temperature rise (9 °C, from 28 to 37 °C), so that a clear and obvious thermal effect could be separated from any non-thermal effect. Our experimental configuration, which also incorporated carefully calibrated EMF E-field and attenuated H-field, showed that while thermal effects did modulate CM Ca^{2+} signalling (Fig. 2, Heat and Fig. 5), only those changes provoked by exposure to 2.4 GHz EMF (i.e., a cumulative thermal and non-thermal effect) elicited increased levels of apoptosis (Figs. 2, 3 and 5).

Previous studies have reported that the abnormal amplification of low amplitude Ca^{2+} fluxes, which do not directly contribute to cellular contractility under normal conditions, had a profoundly negative impact on CM function and survival [26,32,35]. Counter to

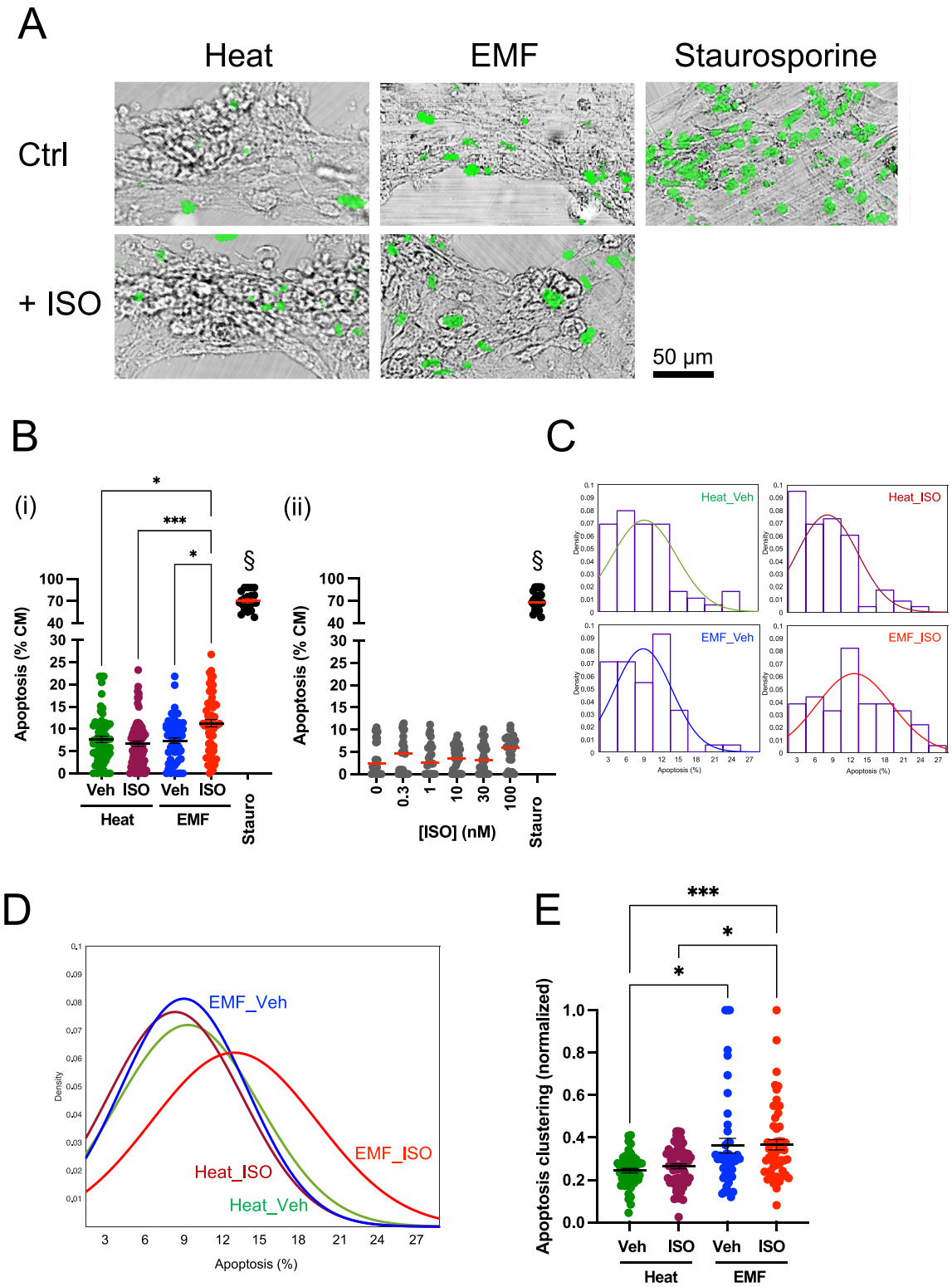

Fig. 3. ISO-stimulation increases apoptosis in CM exposed to 2.4 GHz EMF, but not to heating alone. **(A)** Images of apoptotic nuclei (green) in CM (brightfield) in 'Heat' and 'EMF'-groups under baseline (Baseline) or post-ISO (30 nM, +ISO) conditions. Staurosporine (1 µM, 4 h) was used to provoke the maximum extent of apoptosis. **(B) (i)** Apoptosis in heat- or EMF-exposed CM following the addition of vehicle or ISO. Heat_Veh, N = 63; Heat_ISO, N = 77; EMF_Veh, N = 61; EMF_ISO; N = 61; Staurosporine; N = 21. In **(ii)**, apoptosis in control CM following addition of ISO (0.3–100 nM, 4 h) was measured (N = 20–29). *, $p < 0.05$; ***, $p < 0.001$ between designated groups. §, $p < 0.001$ when compared with any other group.

(C and D) Data from **(B)** plotted in individual histograms **(C)** and combined distributions **(D)**.

(E) Spatial clustering of apoptotic nuclei. Heat_Veh, N = 50; Heat_ISO, N = 61; EMF_Veh. N = 45; EMF_ISO, N = 55. *, $p < 0.05$; ***, $p < 0.001$. N is different from **(B)** since tubular CM structures with none or one TUNEL-stained nucleus cannot be factored into any calculation of CM clustering. (For interpretation of the references to colour in this figure legend, the reader is referred to the Web version of this article.)

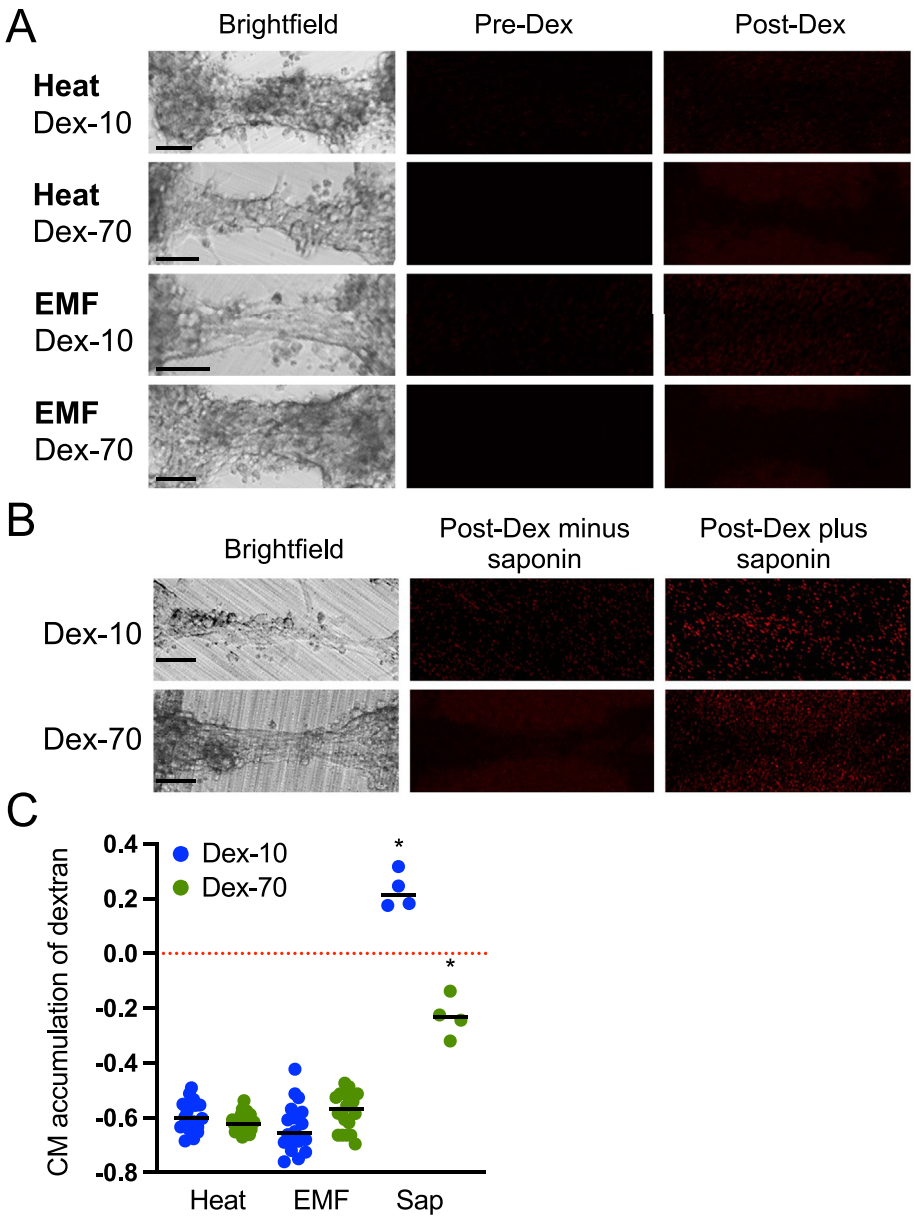

Fig. 4. Heating-only or EMF-exposure does not induce CM surface membrane permeability. **(A)** Representative images of CM tubes before and after incubation with Dex-10 and Dex-70 in 'Heat' or 'EMF'-treated groups (see 2.9 Methods). Scale bar = 50 μm. **(B)** Representative images of the effect of saponin permeabilization (final concentration 0.01% (w/v in L-15 media)) on CM accumulation of Dex-10 and Dex-70. Saponin altered the morphology of some CM tubes under test. Scale bar = 50 μm. **(C)** Ratios <0 and >0 denote intra-CM TMR fluorescence as less than, or more than, fluorescence determined in the bulk media, respectively. Heat_Dex-10, N = 18; Heat_Dex-70, N = 25; EMF_Dex 10, N = 18; EMF_Dex-70, N = 20; Saponin (Sap), N = 4 for both Dex-10 and Dex-70. *$p < 0.05$ when compared with Heat and EMF groups using two-way ANOVA.

these studies that illustrated a pro-apoptotic role for augmented (non-spike) Ca^{2+} fluxes, the data reported in this work evidence a new paradigm in which the *absence* of a β-AR-mediated Ca^{2+} response in CM exposed to 2.4 GHz EMF (Fig. 2) promoted apoptosis (Fig. 3).

The data shown in Fig. 5 confirm that the effects of 2.4 GHz EMF exposure on CM Ca^{2+} signalling are complex. The *similarities* between thermal and non-thermal effects on the relationships between Ca^{2+} signalling parameters in the post-ISO states of 'EMF' and 'Heat' groups illustrates, perhaps, why it has proved difficult so far to untangle the effects of heating- and non-heating components of microwave E-field exposure. However, these data also highlight that the *differences* in Ca^{2+} signalling modulation between heating-only and EMF exposure are likely to be sufficient to underpin the increased apoptotic susceptibility determined in our experiments.

This study was not configured to resolve the specific mechanisms that transduce the impact of EMF exposure into biological perturbations. Formica and Silvestri have advanced the idea that thermal effects arise from *energy* transfer between external EMF sources and cellular material, and that non-thermal effects occur as a consequence of *information* transfer between irradiated cells [39]. On the latter, a dipole effect involving polarized cellular structures [40,41] is entirely consistent with the theory of 'Fröhlich's Condensates' [42,43]. It is possible that vibrational modes of the highly polarized surface membrane of the CM used in this study (membrane potential of approximately −80 mV [26]) might participate in 'information coupling' via resonance interaction with the applied microwave EMF [23,44]. We also speculate that mitochondria could

be involved in mediating the non-thermal effects of 2.4 GHz microwaves. Mitochondria form functionally coupled networks, acting as co-incidence detectors to modulate cellular homeostasis and function [45]. The high charge-separation across mitochondrial membranes might explain the susceptibility of mitochondrial dysfunction to microwave EMF which has been demonstrated by others [18,21,46–49].

Providing mechanistic clarity on how non-thermal effects of microwave EMF disrupt cellular electrical excitability will not be straightforward. For example, measuring the functional impact of microwaves on surface-membrane voltage-gated channels, that are characterised by open-closed kinetics in the nanosecond range, is not possible. There are also practical issues that negate the use of electrophysiologic approaches such as interference caused by the applied microwave E-field on the electronic recording equipment used (e.g. patch clamp).

The intriguing finding that ISO provoked increased levels of spatially-clustered apoptosis in EMF-exposed CM, but not in heat-treated CM, suggests that non-thermal effects of EMF might be variably transduced into biological abnormalities that are predicated by individual CM status in the highly-coupled CM network. It is plausible, but remains to be tested, that the functional uncoupling of sub-populations of damaged CM in these networks might lead to their increased susceptibility to the effects of EMF. This might have relevance therefore to future efforts to develop the therapeutic utility of microwave EMF in targeted destruction of specific sub-populations of cells in damaged tissue (e.g., cellular ablation in post-infarcted myocardium).

5. Study limitations and other considerations

To maximize the likelihood of eliciting a measurable thermal and non-thermal effect on the biological processes that modulate cellular Ca^{2+} signals, our study used microwave power levels equivalent to an absorption of approximately 3 W/g. This is more than 1000-times higher than the recommended specific absorption rate (SAR) safety threshold in Europe and the US. It is unlikely that exposure to microwaves at this power will be encountered in

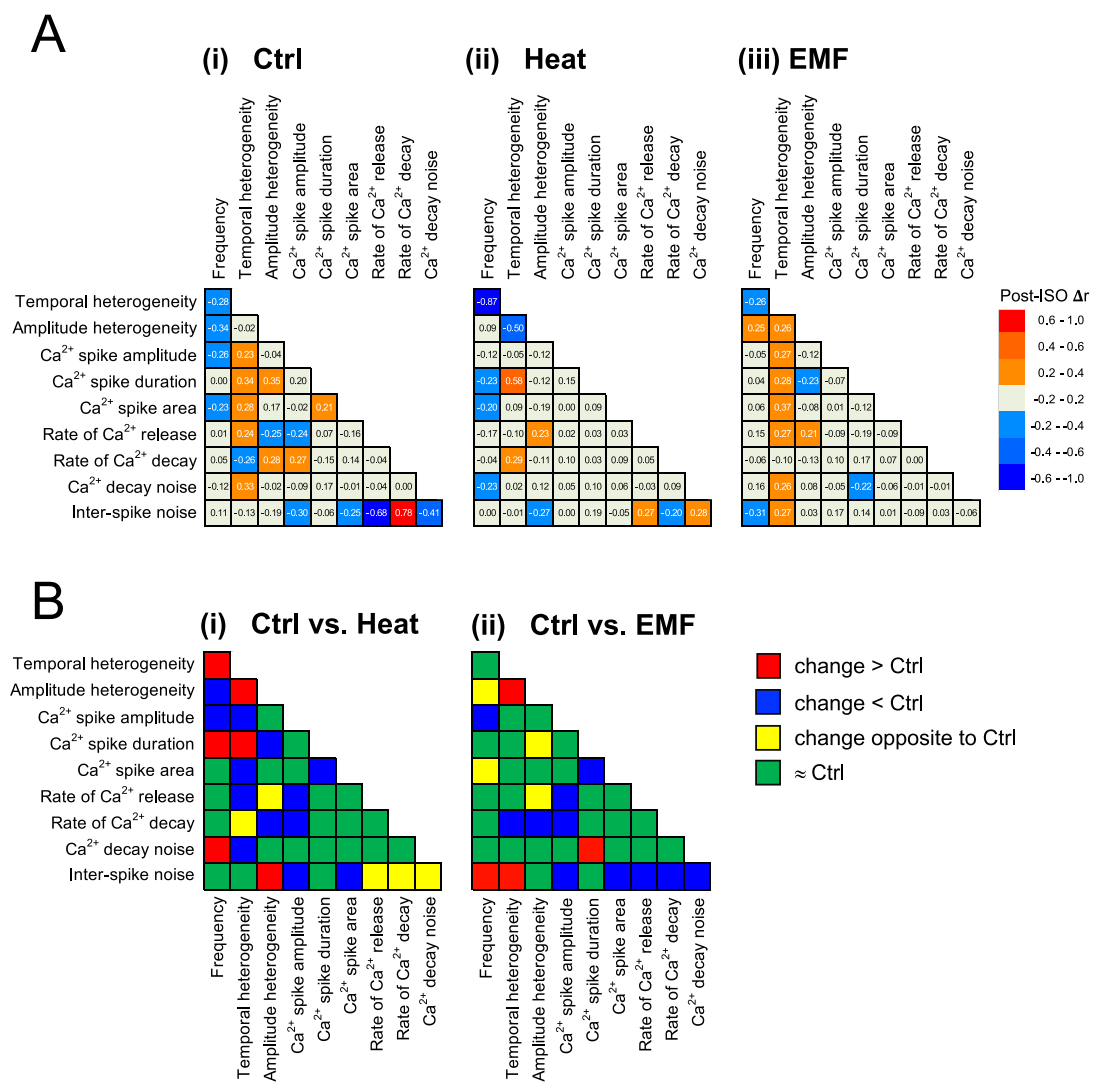

Fig. 5. Different inter-relationships of post-ISO Ca^{2+} signalling in control, Heat-treated or EMF-exposed CM. **(A)** Post-ISO inducedchanges in correlation coefficients (post-ISO Δr) of Ca^{2+} signal descriptors in 'Ctrl', 'Heat' and 'EMF' groups, relative to those determined in the same CM populations under baseline conditions, were calculated. Numeric data are from correlation analysis given in full in Supplementary Fig. 2S, 3S and 4S. The extent of synchronisation (Fig. 2) is calculated from the analysis of multiple intra-tubular regions (see Supplementary Fig. 1S) and was not subject to correlation analysis. **(B)** Post-ISO Ca^{2+} signalling parameter correlations in 'Heat' or 'EMF' groups (Supplementary Figs. 3S and 4S) were plotted relative to those correlations calculated in post-ISO treated control CM (Supplementary Fig. 2S).

everyday life. However, pulses of GHz-frequency microwaves at powers that exceed10W have been used for imaging via thermoacoustic emission [50] and in therapeutic applications, including in the treatment of hypothermia and cancer [51]. The temperature change in both 'Heat' and 'EMF' groups (9 °C acheived at a rate of heating of 0.2 °C/s, Fig. 1E) did not produce measurable increases in the extent of apoptosis (Fig. 4). However, there might be other downstream biological consequences in response to this large thermal gradient that we did not investigate.

In this proof-of-concept work we did not investigate the power-, frequency-, pulse- or time-dependence of EMF effects. Since the perturbation of biological processes might be related to EMF frequency in a highly non-linear manner [39], adding knowledge on these variables will require further work. Microwaves at a frequency of 2.4 GHz were used owing to the relevance of this frequency to 4G communications, Bluetooth™ and WiFi. Next generation communication systems (e.g., 5G and above) will use higher frequencies for greater data bandwidth and gaining new knowledge on the functional impact of these higher frequencies on human health is a priority area for future study.

The data reported in this study show that non-thermal effects of EMF fundamentally remodel β-AR -stimulated Ca^{2+} signalling and lead to increased levels of apoptosis. We recognise though that there might be other downstream consequences of EMF exposure, on aspects of CM behaviour distinct from apoptosis induction, that we did not explore.

We also only exposed CM to microwave E-field since a previous study on the exposure of photoluminescent bacteria to EMF (where light output was used as a biological marker) showed that the magnetic H- field, albeit a necessary component of an electromagnetic wave, had no influence on the state of the bacteria over the full range of microwave power levels used [29]. Whilst our experimental configuration purposely attenuated the applied magnetic H-field therefore, it is conceivable that exceptionally high H-fields might modulate cell and tissue function under some circumstances.

Author contributions

Study conception and design: CFW, DL, AP, CHG.

Experimental work and computer modelling: CFW, CH, CLJ, HC, AP, CHG.

Data and statistical analysis: CFW, CH, JSC, JZ, RGP, AWO, RD, CHG.

Manuscript drafting and editing: CFW, HC, AP, CHG.

Data and resource availability

All raw data and computer code generated in this study is available from the authors upon reasonable request.

Declaration of competing interest

The authors declare the following financial interests/personal relationships which may be considered as potential competing interests: Christopher George reports financial support was provided by British Heart Foundation. Christopher George reports financial support was provided by Wellcome Trust. Christopher George reports financial support was provided by European Union. Adrian Porch reports financial support was provided by Wellcome Trust. Catrin Williams reports financial support was provided by Welsh Government. Heungjae Choi reports financial support was provided by Welsh Government. Christopher George is a Board Member of the National Centre for Replacement, Reduction and Refinement of Animals in Research (NC3Rs) and Chairs the Grants Assessment Panel.

Acknowledgements/Research Funding

The study was supported by a Sêr Cymru II Fellowship part-funded by the European Regional Development Fund through the Welsh Government (TG/KJB/VSM:1063339) to CFW and (TG/KJB/VSM:1103515) to HC; Wellcome Trust Infrastructural Support Fund to CHG and AP; British Heart Foundation Programme Grant (RG/15/6/31436) to CHG; a Swansea University Research Excellence Studentship (SURES) to AWO/CHG; EU/WEFO award to CHG (T37/18).

Appendix A. Supplementary data

Supplementary data to this article can be found online at https://doi.org/10.1016/j.bbrc.2023.04.038.

References

[1] P. Bandara, D.O. Carpenter, Planetary electromagnetic pollution: it is time to assess its impact, Lancet Planet. Health 2 (2018) e512–e514.
[2] I.C.o.N.-I.R.P. (ICNIRP), Guidelines for limiting exposure to electromagnetic fields (100KHz to 300GHz), Health Phys. 118 (2020) 483–524.
[3] T. Wu, T.S. Rappaport, C.M. Collins, Safe for Generations to Come 2015, IEEE Microwave magazine March, 2015, pp. 65–84.
[4] S. Dongus, H. Jalilian, D. S, M. Roosli, Health effects of WiFi radiation: a review based on systematic quality evaluation, Crit. Rev. Environ. Sci. Technol. 52 (2021) 3547–3566.
[5] L. Hardell, M. Carlberg, Health risks from radiofrequency radiation, including 5G, should be assessed by experts with no conflicts of interest, Oncol. Lett. 20 (2020) 15.
[6] M. Simko, M.-O. Mattsson, 5G wireless communication and health effects - a pragmatic review based on available studies regarding 6 to 100 GHz, Int. J. Environ. Res. Publ. Health 16 (2019) 3406.
[7] I.Y. Belyaev, Dependence of non-thermal biological effects of microwaves on physical and biological variables: implications for reproducibility and safety standards, Eur. J. Oncol. Library 5 (2010) 187–217.
[8] S. Dasgupta, G. Wang, M.T. Simonich, T. Zhang, L. Truong, H. Liu, R.L. Tanguay, Impacts of high dose 3.5GHz cellphone radiofrequency on zebrafish embryonic development, PLoS One 15 (2020), e0235869.
[9] W. Ye, F. Wang, W. Zhang, N. Fang, W. Zhao, J. Wang, Effect of mobile phone radiation on cardiovascular development of chick embryo, Anat. Histol. Embryol. 45 (2016) 197–208.
[10] M.H. Bahreyni Toossi, H.R. Sadeghnia, M. Mohammad Mahdizadeh Feyzabadi, M. Hosseini, M. Hedayati, R. Mosallanejad, F. Beheshti, Z. Alizadeh Rahvar, Exposure to mobile phone (900-1800 MHz) during pregnancy: tissue oxidative stress after childbirth, J. Matern. Fetal Neonatal Med. 31 (2018) 1298–1303.
[11] L. Liu, H. Deng, X. Tang, Y. Lu, J. Zhou, X. Wang, Y. Zhao, B. Huang, Y. Shi, Specific electromagnetic radiation in the wireless signal range increases wakefulness in mice, Proc. Natl. Acad. Sci. U.S.A. 118 (2021), e2105838118.
[12] B. Ekici, A. Tanindi, G. Ekici, E. Diker, The effects of the duration of mobile phone use on heart rate variability parameters in healthy subjects, Anatol. J. Cardiol. 16 (2016) 833–838.
[13] O. Elmas, Effects of electromagnetic field exposure on the heart: a systematic review, Toxicol. Ind. Health 32 (2016) 76–82.
[14] R.R. Rekha, J. Sekar, R. Mohan, S.J. Kalpaka, Spectral analysis of heart rate variability during mobile phone usage in first year medical students, International Journal of Physiology 8 (2020) 72–77.
[15] A. Tamer, H. Gunduz, S. Ozyildirim, The cardiac effects of a mobile phone positioned closest to the heart, Anatol. J. Cardiol. 9 (2009) 380, 304.
[16] Y.-S. Lu, B.-T. Huang, Y.-X. Huang, Reactive oxygen species formation and apoptosis in human peripheral blood mononuclear cell induced by 900 MHz mobile phone radiation, Oxid. Med. Cell. Longev. (2012), 740280.
[17] Y.M. Moustafa, R.M. Moustafa, A. Belacy, S.H. Abou-El-Ela, F.M. Ali, Effects of acute exposure to the radiofrequency fields of cellular phones on plasma lipid peroxide and antioxidase activities in human erythrocytes, J. Pharmaceut. Biomed. Anal. 26 (2001) 605–608.
[18] M.A. Esmekaya, C. Ozer, N. Seyhan, MHz pulse-modulated radiofrequency radiation induces oxidative stress on heart, lung, testis and liver tissues, Gen. Physiol. Biophys. 30 (2011) 84–89, 900.
[19] S.K. Dutta, A. Subramoniam, B. Ghosh, R. Parshad, Microwave radiation-induced calcium ion efflux from human neuroblastoma cells in culture, Bioelectromagnetics 5 (1984) 71–78.
[20] V.S. Rao, I.A. Titushkin, E.G. Moros, W.F. Pickard, H.S. Thatte, M.R. Cho, Nonthermal effects of radiofrequency-field exposure on calcium dynamics in stem cell-derived neuronal cells: elucidation of calcium pathways, Radiat. Res. 169 (2008) 319–329.
[21] H. Wang, J. Zhang, S.H. Hu, S.Z. Tan, B. Zhang, H.M. Zhou, R.Y. Peng, Real-time

microwave exposure induces calcium efflux in primary hippocampal neurons and primary cardiomyocytes, Biomed, Environ. Sci. 31 (2018) 561–571.
[22] M.J. Galvin, C.A. Hall, D.I. McRee, Microwave radiation effects on cardiac muscle cells in vitro, Radiat. Res. 86 (1981) 358–367.
[23] R.K. Adair, Biophysical limits on athermal effects of RF and microwave radiation, Bioelectromagnetics 24 (2003) 39–48.
[24] A.S. Dawe, B. Smith, D.W.P. Thomas, S. Greedy, N. Vasic, A. Gregory, B. Loader, D.I. de Pomerai, A small temperature rise may contribute towards the apparent induction by microwaves of heat-shock gene expression in the nematode Caenorhabditis elegans, Bioelectromagnetics 27 (2006) 88–97.
[25] M. Asano, S. Tanaka, M. Sakaguchi, H. Matsumura, T. Yamaguchi, Y. Fujita, K. Tabuse, Normothermic microwave irradiation induces death of HL-60 cells through heat-independent apoptosis, Sci. Rep. 7 (2017), 11406.
[26] K.J. Lewis, N.C. Silvester, S.R. Barberini-Jammaers, S.A. Mason, S.A. Marsh, M. Lipka, C.H. George, A new system for profiling drug-induced calcium signal perturbation in human embryonic stem cell-derived cardiomyocytes, J. Biomol. Screen 20 (2015) 330–340.
[27] C.H. George, D.H. Edwards, Decoding Ca2+ signals as a non-electrophysiological method for assessing drug toxicity in stem cell-derived cardiomyocytes, in: M. Clements, E. Roquemore (Eds.), Stem Cell-Derived Methods in Toxicology, Methods in Pharmacology and Toxicology, Springer, New York, 2017, pp. 173–190.
[28] C.F. Williams, G.M. Geroni, A. Pirog, D. Lloyd, J. Lees, A. Porch, The separated electrical and magnetic field responses of luminescent bacteria exposed to pulsed microwave irradiation, Appl. Phys. Lett. 109 (2016), 093701.
[29] C.F. Williams, G.M. Geroni, D. Lloyd, H. Choi, N. Clark, A. Pirog, J. Lees, A. Porch, Bioluminescence of Vibrio fischeri: bacteria respond quickly and sensitively to pulsed microwave electric (but not magnetic) fields, J. Biomed. Opt. 24 (2019), 051412.
[30] E.K. Ahortor, D. Malyshev, C.F. Williams, H. Choi, J. Lees, A. Porch, L. Baillie, The biological effect of 2.45 GHz microwaves on the viability and permeability of bacterial and yeast cells, J. Appl. Phys. 127 (2020), 204902.
[31] D. Malyshev, C.F. Williams, J. Lees, L. Baillie, A. Porch, Model of microwaves effects on bacterial spores, J. Appl. Phys. 125 (2019), 124701.
[32] A.R. Jones, D.H. Edwards, M.J. Cummins, A.J. Williams, C.H. George, A systemized approach to investigate Ca2+ synchronisation in clusters of human induced pluripotent stem-cell derived cardiomyocytes, Front. Cell Dev. Biol. 3 (2016) 89.
[33] T.-L. Yue, C. Wang, A.M. Romanic, K. Kikly, P. Keller, W.E. DeWolf Jr., T.K. Hart, H.C. Thomas, B. Storer, J.-L. Gu, X. Wang, G.Z. Feuerstein, Staurosporine-induced apoptosis in cardiomyocytes: a potential role of caspase-3, J. Mol. Cell. Cardiol. 30 (1998) 495–507.
[34] T.S. Dhanjal, N. Lellouche, C.J. von Ruhland, G. Abehsira, D.H. Edwards, J.-L. Dubois-Rande, K. Moschonas, E. Teiger, A.J. Williams, C.H. George, Massive accumulation of myofibroblasts in the critical isthmus is associated with ventricular tachycardia inducibility in post-infarct swine heart, J. Am. Coll. Cardiol. Clin. Electrophys. 3 (2017) 703–714.
[35] C.H. George, S.A. Rogers, B.M.A. Bertrand, R.E.A. Tunwell, N.L. Thomas, D.S. Steele, E.V. Cox, C. Pepper, C.J. Hazeel, W.C. Claycomb, F.A. Lai, Alternative splicing of ryanodine receptors modulates cardiomyocyte Ca^{2+} signalling and susceptibility to apoptosis, Circ. Res. 100 (2007) 874–883.
[36] T.H.P. Nguyen, Y. Shamis, R.J. Croft, A. Wood, R.L. McIntosh, R.J. Crawford, E.P. Ivanova, 18 GHz electromagnetic field induces permeability of Gram-positive cocci, Sci. Rep. 16 (2015), 10980.
[37] G.A. Gintant, C.H. George, Introduction to biological complexity as a missing link in drug discovery, Expet Opin. Drug Discov. 13 (2018) 753–763.
[38] D. Tirziu, F.J. Giordano, M. Simons, Cell communications in the heart, Circulation 122 (2010) 928–937.
[39] D. Formica, S. Silvestri, Biological effects of exposure to magnetic resonance imaging: an overview, Biomed. Eng. Online 3 (2004) 11.
[40] D.J. Panagopoulos, O. Johansson, G.L. Carlo, Polarization: a key difference between man-made and natural electromagnetic fields, in regard to biological activity, Sci. Rep. 5 (2015), 14914.
[41] D.J. Panagopoulos, N. Messini, A. Karabarbounis, A.L. Philippetis, L.H. Margaritis, A mechanism for action of oscillating electric fields on cells, Biochem. Biophys. Res. Commun. 272 (2000) 634–640.
[42] H. Frohlich, Long-range coherence and energy storage in biological systems, Int. J. Quant. Chem. 2 (1968) 641–649.
[43] H. Frohlich, The biological effects of microwaves and related questions, Adv. Electronics Electron. Rev. 53 (1980) 85–152.
[44] H. Hinrikus, M. Bachmann, J. Lass, Understandiing physical mechanism of low-level microwave radiation effect, Int. J. Radiat. Biol. 94 (2018) 877–882.
[45] C.F. Williams, C.H. George, Connect and conquer: collectivized behaviour of mitochondria and bacteria, Front. Physiol. 10 (2019) 340.
[46] A.R. Ferreira, F. Bonatto, M.A.B. Pasquali, M. Polydoro, F. Dal-Pizzol, C. Fernandez, A.A.A. de Salles, J.C.F. Moreira, Oxidative stress effects on the central nervous system of rats after acute exposure to ultra high frequency electromagnetic fields, Bio Electro. Mag. 27 (2006) 487–493.
[47] A.M.M. Cermak, I. Pavicic, I. Trosic, Oxidative stress response in SH-SY5Y cells exposed to short-term 1800 MHz radiofrequency radiation, J. Environ. Sci. Health 53 (2018) 132–138.
[48] S. Ni, Y. Yu, Y. Zhang, W. Wu, K. Lai, K. Yao, Study of oxidative stress in human lens epithelial cells exposed to 1.8 GHz radiofrequency fields, PLoS One 8 (2013), e72370.
[49] Y. Turker, Nazuroglu, N. Gumral, O. Celik, M. Saygun, S. Comlekci, M. Flores-Arce, Selenium and L-Carnitine reduce oxidative stress in the heart of rat induced by 2.45-GHz radiation from wireless devices, Biol. Trace Elem. Res. 143 (2011) 1640–1650.
[50] M. Xu, L.V. Wang, Time-domain reconstruction for thermoacoustic tomography in a spherical geometry, IEEE Trans. Med. Imag. 21 (2002) 814–822.
[51] K. Ito, K. Saito, Development of microwave antennas for thermal therapy, Curr. Pharmaceut. Des. 17 (2011) 2360–2366.